



Numerical simulation of thermally developing turbulent flow through a cylindrical tube

Ali Belhocine¹ · Oday Ibraheem Abdullah²

Received: 5 November 2018 / Accepted: 8 January 2019 / Published online: 12 January 2019
© Springer-Verlag France SAS, part of Springer Nature 2019

Abstract

A numerical study was conducted using the finite difference technique to examine the mechanism of energy transfer as well as turbulence in the case of fully developed turbulent flow in a circular tube with constant wall temperature and heat flow conditions. The methodology to solve this thermal problem is based on the energy equation a fluid of constant properties in an axisymmetric and two-dimensional stationary flow. From the mathematical side, a numerical technique for solving the problem of fluid–structure interaction with a fully developed turbulent incompressible Newtonian flow is described. The global equations and the initial and boundary conditions acting on the problem are configured in dimensionless form in order to predict the characteristics of the turbulent fluid flow inside the tube. Using Thomas’ algorithm, a program in FORTRAN was developed to numerically solve the discretized form of the system of equations describing the problem. Finally, using this elaborate program, we were able to simulate the flow characteristics, for changing parameters such as Reynolds, Prandtl and Peclet numbers along the pipe to obtain the important thermal model. These are discussed in detail in this work. Comparison of the results to published data shows that results are a good match to the published quantities.

Keywords Finite difference method · Nusselt number · Fully developed turbulent flow · Reynolds number · Pipe flow

List of symbols

A_j	Coefficient in Eq. (36)	Nu_D	Nusselt number
B_j	Coefficient in Eq. (36)	Nu_{iD}	Local Nusselt number
C_j	Coefficient in Eq. (36)	P	Mean pressure (Pa)
C_p	Specific heat at constant pressure ($J\ kg^{-1}\ K^{-1}$)	Pr	Prandtl number
C_1, C_2	k- ϵ model constants	Pr_t	Turbulent Prandtl number
D	Inner diameter (m)	q_w	Heat transfer rate at the wall
D_j	Coefficient in Eq. (36)	r	Radial coordinate (m)
E	Inner energy ($J\ kg^{-1}$), dimensionless variable	R	Dimensionless radial coordinate
f	Fanning friction factor	Re_D	Reynolds number
F	Function	t	Time (s)
k	Turbulent kinetic energy ($J\ kg^{-1}$)	T	Temperature (K)
L	Tube length (m)	T_b	Bulk temperature (K)
M	Tridiagonal matrix of dimensions ($N \times N$)	T_c	Centerline temperature (K)
		T_i	Initial/entrance temperature (K)
		T_w	Wall temperature (K)
		\bar{T}	Wall temperature (K)
		u_c	Centerline mean velocity ($m\ s^{-1}$)
		u_i	Mean velocity component ($m\ s^{-1}$)
		\bar{u}	Mean velocity ($m\ s^{-1}$)
		\bar{u}_m	Average velocity ($m\ s^{-1}$)
		U	Dimensionless velocity
		\bar{v}	Radial velocity component ($m\ s^{-1}$)
		x_i	Cartesian coordinate (m)

✉ Ali Belhocine
belhocine.2018@gmail.com

¹ Department of Mechanical Engineering, University of Sciences and Technology of Oran, L.P 1505 El -MNAOUER, USTO, 31000 Oran, Algeria

² System Technologies and Mechanical Design Methodology, Hamburg University of Technology, Hamburg, Germany

$y +$	Dimensionless distance from cell center to the nearest wall
z	Axial coordinate (m)
Z	Dimensionless axial coordinate

Greek symbols

α	Thermal diffusivity ($\text{m}^2 \text{s}^{-1}$)
δ_{ij}	Kronecker symbol
ρ	Density of fluid (kg m^{-3})
θ	Dimensionless temperature
ε	Turbulent dissipation rate ($\text{m}^3 \text{s}^{-2}$)
ϵ_h	Eddy viscosity ($\text{kg m}^{-1} \text{s}^{-1}$)
μ	Dynamic viscosity ($\text{kg m}^{-1} \text{s}^{-1}$)
μ_t	Eddy viscosity ($\text{kg m}^{-1} \text{s}^{-1}$)
Φ	Scalar quantities
τ_ω	Wall-shear stress
λ	Thermal conductivity ($\text{W m}^{-1} \text{K}^{-1}$)

Subscripts

i, j, k	Unit direction vector of Cartesian coordinates
local	Local value
out	Outlet
t	Turbulence
wall	Tube wall

1 Introduction

The interaction between a structure and a fluid in which it is submerged or surrounding fluid flow is generally known as Fluid Structure Interaction (FSI). FSI problems exist in numerous applications of engineering such as the stability and response of aircraft wings, the flow of blood through arteries, the response of bridges and tall buildings to wind, the vibration of turbine and compressor blades, the oscillation of heat exchangers. The complexity of current engineering problems leads engineers to model all the elements of their environment with ever greater precision in order to improve the performance of systems [1]. Visual fluid models have many obvious applications in the industry including special effects and interactive games. Ideally, good computer graphics fluid model should both be easy to use and produce highly realistic results. The simulation of a fluid can be split into four main parts: advection, surface tracking, pressure projection and fluid–solid interaction. Each of these parts has been the focus of many research papers. The modeling of fluid flows is essential for mechanics and engineering, especially the fully developed turbulent flow which is the most common flow in

circular pipes. Turbulence is an uncertain, chaotic, unsteady and unpredictable phenomenon [2]. Simulating physically realistic complex fluid behaviors in a distributed interactive simulation (DIS) presents a challenging problem for computer graphics researchers. In many applications, such as simulations involving a dynamic terrain, fluid flow interacts with the environment. Therefore, fluid conservation and the interaction of the flowing fluid with its environment are important issues to address. In addition to high visual quality and stability, simulation algorithms used in interactive applications must have predictable and constant computation time and robustness to all possible user inputs. Recently, Direct Numerical Simulations (DNS) has examined high-speed turbulent mixing layers and the interaction of shock waves with turbulence [3]. The main purpose of DNS is to solve (to best of our ability) for the turbulent velocity field without the use of “turbulent modeling”.

The subject of fluid–structure interaction is immensely vast and can cover almost any field of modern engineering. The main factors, which characterize fluid–structure interaction, are the geometry of the tube, the incompressibility of the fluid and the rigidity of the tube. The numerical solution of the resulting equations of the fluid–structure interaction problem poses great challenges since it includes the features of structural mechanics, fluid dynamics and their coupling. García et al. [4], performed CFD simulation of complex phenomena in batch mode on large high performance computing (HPC) systems. Cucinotta et al. [5], investigated, with a preliminary numerical study by means of Computational Fluid Dynamics (CFD), the Air Cavity Ships technology. Cherad and Benchabane [6] proposed an interactive numerical process to control the evaporating temperature of refrigerant for solar adsorption cooling machine with a new correlation. Bahar et al. [7], presented a CAD transfer method to visualize thermal simulation results in a virtual environment in order to optimize building design determined by energy efficiency. Amaya et al. [8], developed a mathematical and numerical model of flow and combustion process for spark ignition engines using the principles of the first and second law of thermodynamics. Zhang et al. [9], simulated the temperature change of the sinusoidal surface milling process by using the three-dimensional modeling software, Matlab and finite element analysis software.

Afzal [10] analyzed the open equations of thermal turbulent boundary layer subjected to pressure gradient by the method of matched asymptotic expansions at large Reynolds number. Gbadebo et al. [11], developed an empirical correlation for local and average Nusselt numbers in the thermal entrance region of steady and pulsating turbulent air-flows in a pipe. Yan et al. [12], investigated theoretically the turbulent flow in rectangular channels in ocean environment using CFD code FLUENT. Yan et al. [13], investigated theoretically with CFD code FLUENT, the turbulent flow and heat transfer in

triangular rod bundles. Weigand and Wrona [14] analyzed the heat transfer characteristics in the thermal entrance region of concentric annuli for laminar and turbulent internal flow. Habib et al. [15], experimentally investigated heat transfer characteristics to turbulent pulsating pipe flows under a wide range of Reynolds number and pulsation frequency under uniform heat flux condition. Hui and Liejin [16] investigated numerically a three-dimensional turbulent developing flow in a helical square duct with large curvature. Roy et al. [17], conducted a numerical study of turbulent axisymmetric radial compressible channel flow between a nozzle and a flat plate. Eiamsa-ard and Changcharoen [18] also investigated numerically the heat transfers and flow characteristics in a channel with repeated ribs on one broad wall.

Taler [19] analyzed the heat transfers in turbulent pipe flow. Tian et al. [20], analyzed the effects of Prandtl numbers on heat transfers of supercritical pressure fluids. In Taler's later works resulted in a valid engineering model for flows subjected to uniform heat flux through a circular tube [21] for different Reynolds numbers Re Prandtl Pr , of which the number of Nusselt Nu was expressed as a function of friction factor ξ (Re). Belhocine and Wan Omar [22], and Belhocine [23] conducted a study to investigate the distribution of temperature in the pipes for a fully developed laminar flow. More recently, Belhocine and Wan Omar [24] solved the problem of convective heat transfers in circular pipes, whose solutions were in the form of the hypergeometric series. Belhocine and Abdullah [25] then used a similarity solution and Runge–Kutta method to visualize analytically the thermal boundary layer in the vicinity of the inlet of the circular pipe.

In this paper, a two-dimensional heat transfer in a fully developed turbulent flow in a circular duct is numerically investigated. The work utilizes a FORTRAN code which applied the finite difference method to solve thermal problems on two boundary conditions. The situation is relevant as an asymptotic case in several application fields in engineering design, as heat transfer and chemical catalysis. The interaction between a simple circular conduit and a fluid flow under turbulent, well-defined, uniform and fully developed inlet and outlet flow conditions was investigated. The work consisted of studies with constant wall temperature and surface heat flux with fully turbulent axisymmetric flow. The numerical results of the model were validated by comparing them with some results available in specialized literatures. The comparisons give good agreements with published data.

2 The flow governing equations

In a flow, the governing equations are the continuity, momentum and energy equations:

$$\frac{\partial(\rho u_i)}{\partial x_i} = 0 \quad (1)$$

$$\begin{aligned} \frac{\partial}{\partial t}(\rho u_i) + \frac{\partial}{\partial x_j}(\rho u_i u_j) \\ = -\frac{\partial P}{\partial x_i} + \frac{\partial}{\partial x_j} \left[\mu \left(\frac{\partial u_i}{\partial x_j} + \frac{\partial u_j}{\partial x_i} - \frac{2}{3} \delta_{ij} \frac{\partial u_j}{\partial x_i} \right) \right] \\ + \frac{\partial}{\partial x_j} \left(-\rho \overline{u'_i u'_j} \right) \end{aligned} \quad (2)$$

$$\begin{aligned} \frac{\partial}{\partial x_i} [u_i (\rho E + P)] \\ = \frac{\partial}{\partial x_i} \left[\left(\lambda + \frac{c_p \mu_t}{Pr_t} \right) \frac{\partial T}{\partial x_j} + \mu \mu_t \left(\frac{\partial u_i}{\partial x_j} + \frac{\partial u_j}{\partial x_i} - \frac{2}{3} \delta_{ij} \frac{\partial u_j}{\partial x_i} \right) \right] \end{aligned} \quad (3)$$

where λ is the thermal conductivity and E is the total energy expressed by.

$$E = c_p T - P/\rho + u^2/2$$

From the momentum equation a transport equation for the Reynolds stress tensor can be derived [26] as

$$\frac{\partial(\rho \overline{u'_i u'_j})}{\partial t} + C_{ij} = D_{T,ij} + D_{I,ij} + P_{ij} + \Phi_{ij} + \varepsilon_{ij} \quad (4)$$

where C_{ij} , $D_{T,ij}$, $D_{I,ij}$, P_{ij} , Φ_{ij} and ε_{ij} are respectively the terms of convection, turbulent diffusion, molecular diffusion, shear stress production, stress–strain and viscosity dissipation.

$$C_{ij} = \frac{\partial}{\partial x_k} (\rho u_k \overline{u'_i u'_j}) \quad (5)$$

$$D_{T,ij} = -\frac{\partial}{\partial x_k} (\rho \overline{u'_i u'_j u'_k} + \overline{P' u'_i} \delta_{kj} + \overline{P' u'_j} \delta_{ik}) \quad (6)$$

$$D_{I,ij} = \frac{\partial}{\partial x_k} \left[\mu \frac{\partial}{\partial x_k} (\overline{u'_i u'_j}) \right] \quad (7)$$

$$P_{ij} = -\rho \left(\overline{u'_i u'_k} \frac{\partial u_j}{\partial x_k} + \overline{u'_j u'_k} \frac{\partial u_i}{\partial x_k} \right) \quad (8)$$

$$\Phi_{ij} = P' \left(\frac{\partial u'_i}{\partial x_j} + \frac{\partial u'_j}{\partial x_i} \right) \quad (9)$$

$$\varepsilon_{ij} = -2\mu \frac{\partial u'_i}{\partial x_k} \frac{\partial u'_j}{\partial x_k} \quad (10)$$

For computational stability, $D_{T,ij}$, $\Phi_{T,ij}$ and $\varepsilon_{T,ij}$ which are defined as follows.

$$D_{T,ij} = \frac{\partial}{\partial x_k} \left(\frac{\mu_t}{\sigma_k} \frac{\partial \overline{u'_i u'_j}}{\partial x_k} \right) \quad (11)$$

where $\sigma_k = 0.82$ and μ_t is the turbulent viscosity, and

$$\phi_{ij} = \phi_{ij,1} + \phi_{ij,2} + \phi_{ij,w} \quad (12)$$

with $\phi_{ij,w}$, $\phi_{ij,1}$ and $\phi_{ij,2}$ are respectively the surface reflection term, slow term, and the rapid term. The last two terms are defined as follows

$$\phi_{ij,1} = -C_1 \rho \frac{\varepsilon}{k} \left(\overline{u_i' u_j'} - \frac{2}{3} \delta_{ij} k \right) \quad (13)$$

$$\phi_{ij,2} = -C_2 \left(P_{ij} - \frac{2}{3} P \delta_{ij} \right) \quad (14)$$

where $C_1 = 1.8$ and $C_2 = 0.6$.

As for the viscosity dissipation, the large-scale vortex is essentially engaged in the transport of momentum. Nevertheless, it was considered that dissipation was generated only in a small-scale isotropic vortex. So the equation for ε_{ij} has been reduced to the following expression

$$\varepsilon_{ij} = \frac{2}{3} \rho \varepsilon \delta_{ij} \quad (15)$$

3 Simplifying assumptions used in the turbulent flow analysis

The governing equations for convective heat transfer flow as presented above together form a very complex set of simultaneous partial differential equations. Analytical solutions to this set of equations could be realized for a few, relatively very simple cases. Numerical solutions for these equations for three-dimensional flow solutions may be relatively large and would require substantial computer resources.

The following two types of flow are, from a practical viewpoint, are probably the most important. For these two flows, some simplifying assumptions can be adopted.

In the case of flow inside a duct, it can be assumed that the flow is fully developed. Basically, this means that it can be assumed that certain properties of the flow do not change with

distance along the duct. Real duct flows well away from the entrance or other fittings could be said to be fully developed. Understanding the entrance length is important for the design and analysis of flow systems. The entrance region will have different velocity, temperature, and other profiles than exist in the fully developed region of the pipe.

For fully developed duct flows, it can be assumed that the fluid properties are constant, and the form of the velocity and temperature profiles does not change with distance along the duct. Such a condition could be presented in Fig. 1. If the velocity and temperature profiles are expressed in the form, then in fully developed flow, the velocity and temperature profile functions f and g are independent of the distance along the duct.

$$\left(\frac{u}{u_c} \right) = f\left(\frac{r}{D}\right), \quad \left(\frac{T - T_c}{T_w - T_c} \right) = g\left(\frac{r}{D}\right) \quad (16)$$

This means that the velocity at any distance y from the center line of the duct remains constant with distance along the duct, and that the temperature at the same position, will vary relative to the center line and wall temperatures.

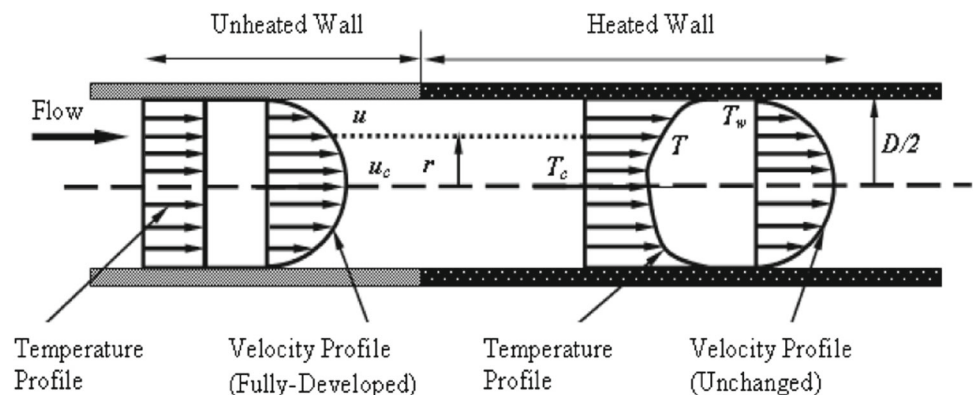
As such $(T - T_c)/(T_w - T_c)$ remains constant. In fully developed flow, since u does not change, it follows that the velocity components in the radial and tangential directions will be zero.

4 Numerical procedure of the thermal problem

4.1 Thermally developing pipe flow

In this analysis, there is initially no thermal transfer until the flow is fully developed. Then only the heat transfer would begin, but the properties of the fluid are initially assumed to be constant [27]. Thus, the velocity field will not vary in this region. In our simulation, we had limited the thermal problem to the case of constant fluid properties, such that the

Fig. 1 Thermally developing pipe flow




```

C *****
C
C      SUBROUTINE TRISOL(A,B,C,D,H,N)
C
C ***** TRI-DIAGONAL MATRIX SOLVER *****
C
C *** THIS TRIDIAGONAL MATRIX SOLVER USES THE THOMAS ALGORITHM *****
C
dimension A(250),B(250),C(250),D(250),H(250),W(250),R(250),G(250)
W(1)=A(1)
G(1)=D(1)/W(1)
do 100 I=2,N
  I1=I-1
  R(I1)=B(I1)/W(I1)
  W(I)=A(I)-C(I)*R(I1)
  G(I)=(D(I)-C(I)*G(I1))/W(I)
100 continue
H(N)=G(N)
N1=N-1
do 200 I=1,N1
  II=N-I
  H(II)=G(II)-R(II)*H(II+1)
200 continue
return
end
    
```

Fig. 2 Subroutine Thomas written in FORTRAN 95

And

$$d'_1 = \frac{d_1}{b_1} \tag{30}$$

$$d'_i = \frac{d_i - a_i d'_{i-1}}{b_i - a_i c'_{i-1}} \text{ for } i = 2, 3, \dots, N \tag{31}$$

The unknowns u_1, u_2, \dots, u_N are then obtained by the formulas:

$$u_N = d'_N \tag{32}$$

$$u_i = d'_i - c'_i u_{i+1} \text{ for } i = N - 1, N - 2, \dots, 2, 1 \tag{33}$$

In CFD solution techniques, the algorithm in question is directly coded in the resolution process in contrast to machine-optimized subroutines that are used on a specific computer. A simple example of a FORTRAN program to adapt this algorithm is well illustrated in Fig. 2.

4.5 The numerical method

Notice that the variations of the quantities U and E with R are known, as long as the fluid velocity is fully developed.

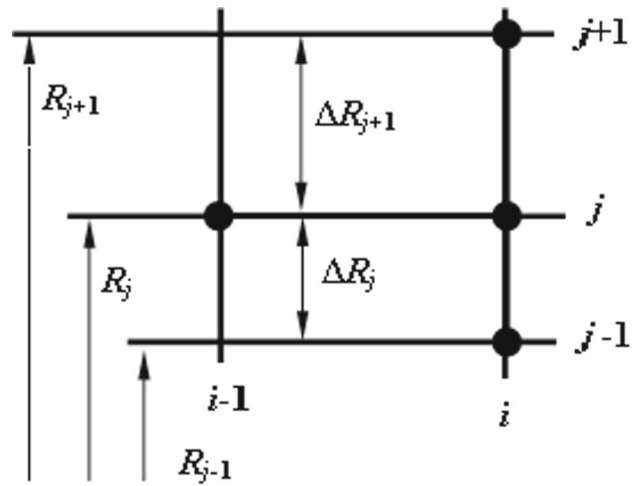


Fig. 3 Nodal points used in obtaining finite-difference solution

The equation obtained will now be processed numerically by the finite difference method since it is better adapted to a medium with a wall temperature that varies according to the longitudinal coordinate Z. This method is simple in its concept but effective in its results, as such it is often used in heat transfer problems.

Figure 3 represents the nodal points used in the numerical simulation. Here, the finite difference method of approximations is introduced, and an explicit backward order of order 1 in the direction (i) is used where the variable U does not change, to evaluate values at the spatial coordinate (Z).

$$U \frac{\partial \theta}{\partial Z} \Big|_{i,j} = U_j \left[\frac{\theta_{i,j} - \theta_{i-1,j}}{\Delta Z} \right] \tag{34}$$

$$\frac{1}{R} \frac{\partial}{\partial R} \left[R \left(E \frac{Pr}{Pr_T} + 1 \right) \frac{\partial \theta}{\partial R} \right] \Big|_{i,j} = \frac{1}{R_j} \frac{2}{\Delta R_{j+1} + \Delta R_j} \times \left\{ \left[\frac{R_{j+1}(E_{j+1} Pr / Pr_T + 1) + R_j(E_j Pr / Pr_T + 1)}{2} \right] \left(\frac{\theta_{i,j+1} - \theta_{i,j}}{\Delta R_{j+1}} \right) - \left[\frac{R_j(E_j Pr / Pr_T + 1) + R_{j-1}(E_{j-1} Pr / Pr_T + 1)}{2} \right] \left(\frac{\theta_{i,j} - \theta_{i,j-1}}{\Delta R_j} \right) \right\} \tag{35}$$

By replacing the derivatives by its finite difference approximations obtained from Eq. (23), we obtain an equation in the following form:

$$A_j \theta_{i,j} + B_j \theta_{i,j+1} + C_j \theta_{i,j-1} = D_j \tag{36}$$

The coefficients A_j, B_j, C_j and D_j resulting from the calculations are obtained from the mining form

$$A_j = \frac{U_j}{\Delta Z} + \frac{1}{R_j} \frac{2}{\Delta R_{j+1} + \Delta R_j} \times \left\{ \left(\frac{1}{\Delta R_{j+1}} \right) + \left[\frac{R_{j+1}(E_{j+1} Pr / Pr_T + 1) + R_j(E_j Pr / Pr_T + 1)}{2} \right] \times \left[\frac{R_j(E_j Pr / Pr_T + 1) + R_{j-1}(E_{j-1} Pr / Pr_T + 1)}{2} \right] \left(\frac{1}{\Delta R_j} \right) \right\} \tag{37}$$

$$B_j = -\frac{1}{R_j} \frac{2}{\Delta R_{j+1} + \Delta R_j} \times \left\{ \left[\frac{R_{j+1} (E_{j+1} Pr / Pr_T + 1) + R_j (E_j Pr / Pr_T + 1)}{2} \right] \left(\frac{1}{\Delta R_{j+1}} \right) \right\} \tag{38}$$

$$C_j = -\frac{1}{R_j} \frac{2}{\Delta R_{j+1} + \Delta R_j} \times \left\{ \left[\frac{R_j (E_j Pr / Pr_T + 1) + R_{j-1} (E_{j-1} Pr / Pr_T + 1)}{2} \right] \left(\frac{1}{\Delta R_j} \right) \right\} \tag{39}$$

$$D_j = \frac{U_j \theta_{i-1,j}}{\Delta Z} \tag{40}$$

Insertion of boundary conditions into the equations for this problem leads to $\theta_{i,2} = \theta_{i,1}$ and $\theta_{i,N} = 1$. By exploiting this boundary conditions and applying at all “internal” points ($j = 1, 2, 3, \dots, N - 2, N - 1$) in Eq. (36), a system of N equations for N unknown θ could be summarized in the following form.

$$\begin{aligned} \theta_{i,1} - \theta_{i,2} &= 0 \\ A_2 \theta_{i,2} + B_2 \theta_{i,3} + C_2 \theta_{i,1} &= D_2 \\ A_3 \theta_{i,3} + B_3 \theta_{i,4} + C_3 \theta_{i,2} &= D_3 \\ A_4 \theta_{i,4} + B_4 \theta_{i,5} + C_4 \theta_{i,3} &= D_4 \\ &\vdots \\ A_{N-1} \theta_{i,N-1} + B_{N-1} \theta_{i,N} + C_{N-1} \theta_{i,N-2} &= D_{N-1} \\ \theta_{i,N} &= 1 \end{aligned} \tag{41}$$

Or in matrix form

$$\begin{bmatrix} 1 & -1 & 0 & 0 & 0 & \dots & 0 & 0 & 0 \\ C_2 & A_2 & B_2 & 0 & 0 & \dots & 0 & 0 & 0 \\ 0 & C_3 & A_3 & B_3 & 0 & \dots & 0 & 0 & 0 \\ 0 & 0 & C_4 & A_4 & B_4 & \dots & 0 & 0 & 0 \\ \vdots & \vdots & \vdots & \vdots & \vdots & \ddots & \vdots & \vdots & \vdots \\ 0 & 0 & 0 & 0 & 0 & \dots & C_{N-1} & A_{N-1} & B_{N-1} \\ 0 & 0 & 0 & 0 & 0 & \dots & 0 & 0 & 0 \end{bmatrix} \times \begin{bmatrix} \theta_{i,1} \\ \theta_{i,2} \\ \theta_{i,3} \\ \theta_{i,4} \\ \vdots \\ \theta_{i,N-1} \\ \theta_{i,N} \end{bmatrix} = \begin{bmatrix} 0 \\ D_2 \\ D_3 \\ D_4 \\ \vdots \\ D_{N-1} \\ 1 \end{bmatrix} \tag{42}$$

$$Q \theta_{i,j} = R \tag{43}$$

where Q is a tridiagonal matrix. This can be effectively solved by Thomas’s algorithm for tridiagonal matrix. For any value of Z , we can estimate the local heat transfer rate as follows:

$$q_\omega = k \left. \frac{\partial \bar{T}}{\partial r} \right|_{r=R} \tag{44}$$

where q_ω is derived from

$$\frac{q_\omega D}{k(T_\omega - T_i)} = \left. \frac{\partial \theta}{\partial R} \right|_{R=0.5} \tag{45}$$

This implies that

$$Nu_{iD} = \left. \frac{\partial \theta}{\partial R} \right|_{R=0.5} \tag{46}$$

where Nu_{iD} is the local number. Then

$$Nu_{iD} = \frac{q_\omega D}{k(T_\omega - T_i)}. \tag{47}$$

However

$$\left. \frac{\partial \theta}{\partial R} \right|_{i,1} = \frac{\theta_{i,N} - \theta_{1,N-1}}{\Delta R_N}, \tag{48}$$

which means replacing Eq. (48) into Eq. (46) would result in

$$Nu_{iD} = \frac{\theta_{i,N} - \theta_{1,N-1}}{\Delta R_N} \tag{49}$$

This Nusselt number is based on the spacing between wall temperatures and local average temperatures, the flow via the pipe is practically considered, so we draw

$$Nu_D = \frac{q_\omega D}{k(T_\omega - \bar{T}_m)} = \frac{q_\omega D}{k} Nu \tag{50}$$

where Nu is the averaged local Nusselt number. This can be expressed as $Nu = \frac{1}{T_\omega - \bar{T}_m}$.

Substituting Eq. (47) into Eq. (50), allows us to write

$$Nu_D = Nu_{iD} \frac{T_\omega - T_i}{T_\omega - \bar{T}_m} = \frac{Nu_{iD}}{\theta_m} \tag{51}$$

with

$$\theta_m = \frac{T_\omega - \bar{T}_m}{T_\omega - T_i}. \tag{52}$$

We can then define the bulk temperature through the tube which is the temperature of the fluid that can be calculated by

$$T_b = \frac{\int_0^{D/2} \rho 2\pi r dr \bar{u} c_p \bar{T}}{\int_0^{D/2} \rho 2\pi r dr \bar{u} c_p} \tag{53}$$

In this expression, the denominator indicates the multiplication of the specific heat integrated in the flow zone with the mass flow, while the numerator indicates that the total

energy flowing through the tube. This results in the following expression

$$\bar{T}_m = \frac{\int_0^{D/2} \bar{u} \bar{T} r dr}{\int_0^{D/2} \bar{u} r dr} \tag{54}$$

which can be written as

$$\theta_m = \int_0^{0.5} U \theta R dR / \int_0^{0.5} U R dR. \tag{55}$$

By using a pre-determined numeric value of θ with R for any value of Z , the values θ_m can be drawn. So, we can determine the value of Nu_D at this value of Z .

The solution to this problem can then be obtained such that, we must specify the variations of U and $E = (\epsilon/\nu_c/\nu)$ in which the distribution of E is given by the following equations

$$\begin{aligned} y^+ < 5 : E &= 0 \\ 5 \leq y^+ \leq 30 : E &= \frac{y^+}{5} - 1 \\ y^+ > 30 : E &= 1.6R(y^+)^{6/7} - 1 \end{aligned} \tag{56}$$

with

$$y^+ = \frac{y}{\nu} \sqrt{\frac{\tau_w}{\rho}} = (0.5 - R) Re_D \sqrt{\frac{f}{8}}$$

in which f is the friction factor

$$f = \frac{0.305}{Re_D^{0.25}}. \tag{57}$$

This is valid for hydraulically smooth pipe with turbulent flow up to the Reynolds number $10^5 (Re < 10^5)$ giving

$$\frac{\bar{u}}{u_c} = \left(\frac{D - 2r}{D} \right)^{1/7} \tag{58}$$

where \bar{u}_c means the center line speed. Now the value of \bar{u}_m becomes

$$\bar{u}_m = \frac{8}{D^2} \int_0^{D/2} \bar{u} r dr \tag{59}$$

which tends towards

$$\frac{\bar{u}_m}{\bar{u}_C} = 8 \int_0^{0.25} (1 - 2R)^{1/7} R dR = \frac{49}{60}. \tag{60}$$

By comparing the two equations, we can draw the following result

$$U = \frac{49}{60} (1 - 2R)^{1/7}. \tag{61}$$

This equation finally yields the average values of the dimensionless velocity U as a function of the radius of tube R . A program in FORTRAN 95 was used to solve the thermal values in fully developed turbulent flow inside a cylindrical tube with uniform wall temperature. The program was based on the finite difference method.

5 Results and discussions

5.1 Uniform wall temperature

The average Nusselt number Nu_D along the pipe is shown in Fig. 4 for different Reynolds number Re_D at Prandtl number $Pr = 0.7$. The Nu number helps to determine whether the flow is hydrodynamically fully developed, or otherwise. The decrease in Nu for $Re = 100000$ to 50000 is very significant such that it suggests different flow regimes occurred at these two Reynolds number values. There is also a high gradient of Nu changes for axial positions near the entrance to the tube. These high gradients are caused by high friction in the flow near the entrance to the pipe.

Using the results obtained from the calculation codes, the the Nusselt number variations for different Prandtl numbers are plotted against the pipe axial position as shown in Fig. 5. From an approximation of the distances from the tube thermal entrance, it has been found that variations in Prandtl number has significant effects on the Nusselt number values. This distance is defined as the thermal entrance length, which is

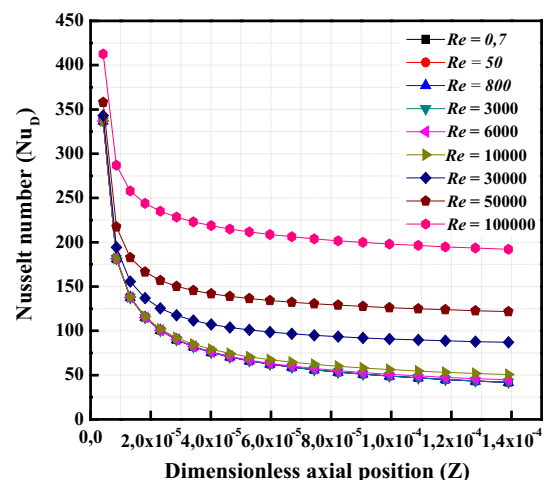


Fig. 4 Variation of Nusselt number Nu_D for $Pr = 0.7$ at the thermal input entrance region and various values of Re_D

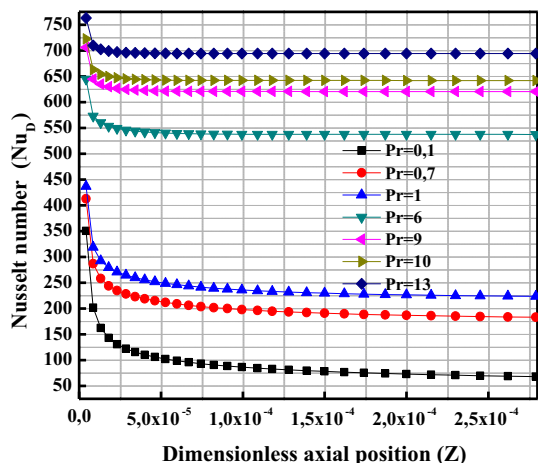


Fig. 5 Variation of Nusselt number Nu_D in the thermal entrance region for $Re_D = 10^5$ for various values of Pr

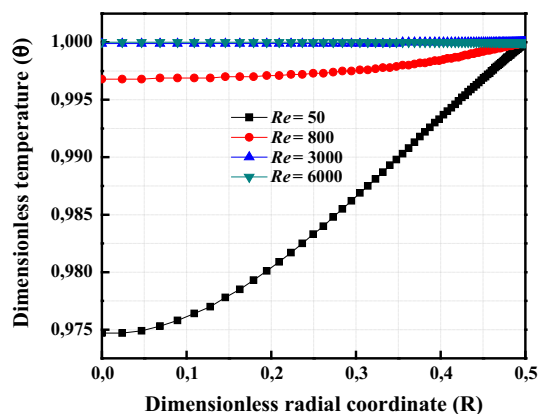


Fig. 6 Dimensionless temperature profile (θ) along radial coordinate for different values of Reynolds numbers

important for engineers to design efficient heat transfer processes. In fact, although it is hard to see in the presented scale, different Prandtl values also yielded different Nu values for the isothermal wall condition.

Dimensionless temperature results are plotted against dimensionless radial positions for the constant wall temperature case, for Reynolds numbers 50, 800, 3000, and 6000, are presented in Fig. 6. Figure 6 shows that when the Reynolds number is low, the temperature of the fluid varied markedly from the centre of the tube (equal to the inlet temperature) to the wall. This variation reduces as the Re is increased, to equal the wall temperature when as Re reaches 3000. Re being the ratio of inertial to frictional forces, which is related to the viscosity of the fluid, would increase gradually as the temperature of the heating fluid increases from the inlet values to the wall temperature values.

The dimensionless axial velocity profile, as a function of radial position for turbulent flow at Prandtl number $Pr = 0.7$

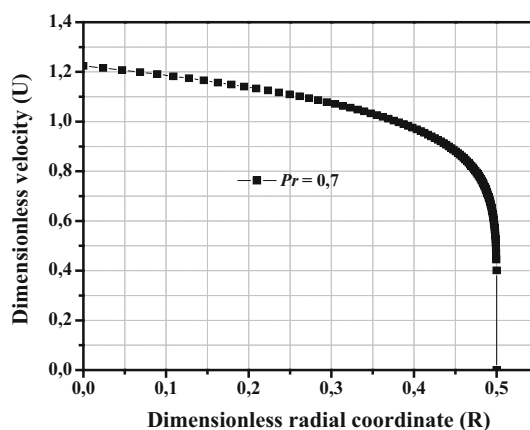


Fig. 7 Dimensionless axial velocity profile (U) for $Pr = 0.7$

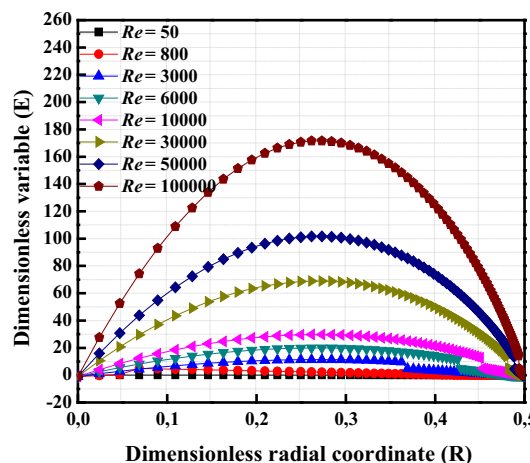


Fig. 8 Dimensionless eddy viscosity distribution (E) along the dimensionless radius (R) for $Pr = 0.7$ for various Reynolds numbers of the flow

is depicted in Fig. 7. Fully developed laminar flow would produce the parabolic profile, while a turbulent flow would produce a much steeper slope near the wall. The axial velocity is maximum at the centerline and gradually decreases towards the wall, and as it nears the wall (dimensionless radius of 0.45) it reduces sharply to satisfy the no-slip boundary condition for viscous flow. This effect is a slight decrease of the shear stresses at the wall and an overall decrease of the pressure-drop.

The dimensionless eddy viscosity distribution (E) along the dimensionless radius of the pipe at different values of the Reynolds numbers (Re) is shown in Fig. 8. It can be seen that the dimensionless eddy viscosity profiles also have a more uniform and almost coincide with the symmetric parabolic distribution. The concavity of this parabola varies with the Reynolds number. We see a significant change in maximum eddy viscosity towards the central part of the pipe at Reynolds number values above 6000. The turbulent regime begins in

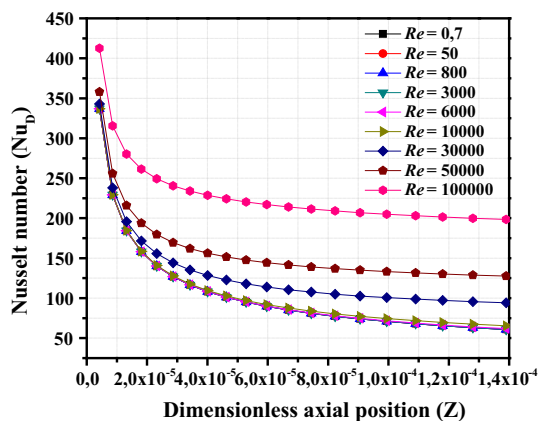


Fig. 9 Variation of Nusselt number Nu_D in thermal entrance region for $Pr = 0.7$ for various values of Re_D

the pipe ($Re > 4000$). Indeed, the turbulent flow consists of eddies of various size ranges, which increase with increasing Reynolds number. The kinetic energy of the flow would cascade down from large to small eddies of interactional forces between the eddies.

5.2 Wall heat flux uniform

Figure 9 shows the Nusselt number variations at the thermal entrance region for $Pr = 0.7$ plotted for different values of Re_D in the case of uniform wall heat flux, in order to represent the augmentation in the heat transfer.

It can be seen that as Re increases above 10,000 the average Nusselt number for the circular tube starts to increase significantly. Axially the Nu values decreased rapidly from the entrance to a point of about $Z = 5 \times 10^{-5}$, after which the reduction is of lower and constant values as shown with the straight line graphs. The straight lines also show that the turbulent flow is fully developed. The development of the turbulent flow is significantly affected by the large Reynolds number values.

Nusselt number Nu_D variations with axial variations at Reynolds number 6000 and Prandtl number 0.7 as obtained from the program codes for fully developed turbulent flow in the tube with constant wall heat flux are shown in Table 1.

The dimensionless temperature profiles along the dimensionless radius are plotted in Fig. 10 for Prandtl number 0.7 and various Reynolds numbers. Note that the effects of increasing the Reynolds number is to give a more “square” temperature profile, while a low Reynolds number yields a more rounded profile similar to that of laminar flow. As the Reynolds number increases to more than 3000 the dimensionless temperatures approach a constant value of 0.8, except at points near the wall of the tube.

Table 1 Summarized results of the FORTRAN 95 code for uniform wall heat flux for $Re = 6000$ and $Pr = 0.7$

Z	T_{Wall}	Nu_{Di}	Nu_{Da}
0.0000042	0.003	334.9473	336.8423
0.0000086	0.0044	227.3414	229.1351
0.0000132	0.0055	182.6194	184.4026
0.0000181	0.0064	156.3688	158.1592
0.0000232	0.0072	138.4781	140.2811
0.0000286	0.008	125.2165	127.0338
0.0000342	0.0087	114.8419	116.6743
0.0000401	0.0094	106.4161	108.2639
0.0000463	0.0101	99.3814	101.245
0.0000528	0.0107	93.3841	95.2636
0.0000597	0.0113	88.1857	90.0813
0.0000669	0.012	83.6188	85.5309
0.0000744	0.0126	79.5622	81.4912
0.0000823	0.0132	75.9255	77.8718
0.0000906	0.0138	72.6394	74.6036
0.0000994	0.0144	69.6501	71.6326
0.0001085	0.0149	66.915	68.9166
0.0001182	0.0155	64.3988	66.42
0.0001283	0.0161	62.0737	64.1152
0.0001389	0.0167	59.9168	61.9793
0.0001500	0.0173	57.9081	59.9923

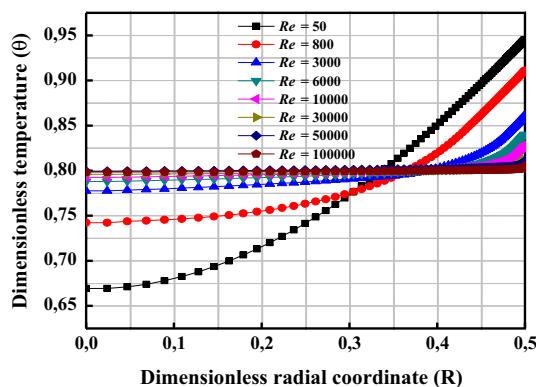


Fig. 10 Temperature behavior (θ) versus dimensionless radius (R) for various values of Reynolds number

5.3 Comparison of constant wall temperature and heat flux cases

The calculations of the heat transfers in fully developed turbulent flow inside a circular pipe, the Nusselt numbers results for the case of constant wall temperature and the case of constant heat flux at constant Reynolds number of 104 (shown in Fig. 11) are compared. The Nusselt numbers in the case of uniform wall temperature are more than the numbers for wall in uniform heat flux. This Nu values decreased sharply exponentially at the entrance but as the flow moved away

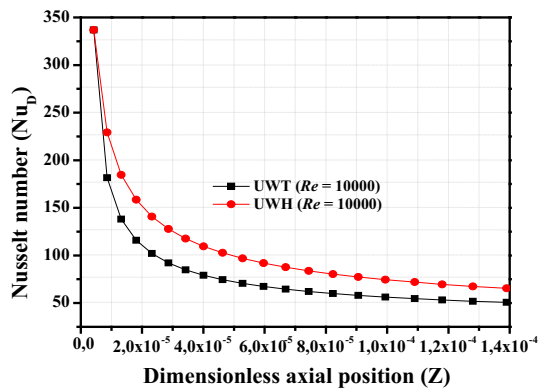


Fig. 11 Comparison of Nu profile along the pipe for uniform wall temperature (UWT) and constant heat flux (UWH) for $Re = 10,000$

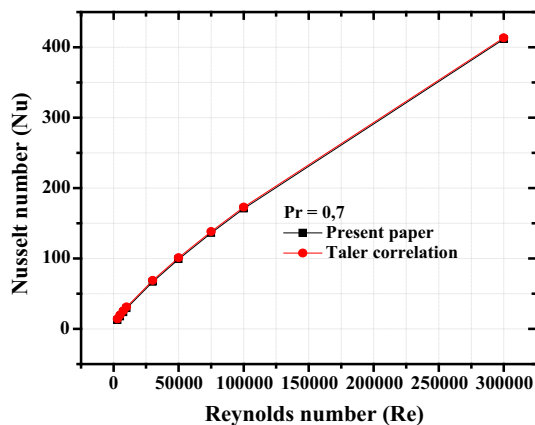


Fig. 12 Comparison of the results from the present work to those from Taler [21] for turbulent air flow in circular tube with constant wall heat flux

from the entrance, the Nu decreased at lower rates, resulting in two distinct values for the two thermal cases.

5.4 Comparison of the present numerical model to previously published data

The results of this thermal problem simulation are compared to the work recently performed by Taler [21] using the finite difference method. Taler evaluated the Nu variations with Re for different Prandtl numbers. In addition, Nu were obtained for fully developed turbulent flow in tubes with constant wall heat flux after solving the energy conservation equation.

The variations of the Nu to Re for $Pr = 0.7$ from this work were compared to the results of Taler and shown in Fig. 12. The two results matched very well, with variations of not more than 2%. This shows that the model used in this work is verified and validated, and thus confirms the reliability of the numerical method and model for turbulent flow inside a circular tube used in this work.

6 Conclusions

The impact of our contribution on the prediction of the heat transfer rate at the wall of a pipe towards a fluid in turbulent flow is presented. Main attention was given to two dimensional and axi-symmetric flows through circular pipes. The analysis is based on the thermal equations of turbulent flow models which was solved using finite-difference method. The equations were adapted for any thermal boundary conditions, so long as the velocity profile is fully developed at the point where heat transfer starts. A FORTRAN program simulating the fully developed turbulent fluid flow through a circular tube, together with heat flow model, was developed. The program was then used to analyze two thermal boundary conditions of uniform wall temperature and constant heat flux. It was found that the surface temperature is higher with higher Reynolds numbers, due to the free convection dominant in the combined heat transfer process. The mean axial velocity and temperature profiles were found to increase and extend farther in the outer layer with increasing Reynolds numbers. This consequently made the local Nu numbers to be higher for high Re numbers. This is due to the forced convection that dominates the heat transfer process. The thermal flux results show the influences and sensitivities of some of the parameters involved in the calculations. The results obtained agree well with available literature with uncertainties of less than 2%. In the fully developed turbulent flow, the Nusselt number, as well as the dimensionless temperatures increase with increasing Reynolds numbers.

The results of Nu were also compared to published results,

It is also necessary to compare the numerical results of this work, especially the Nusselt numbers variations, temperature and velocity profiles with experimental data, but this could be done for now for the lack of the said data.

It should also be mentioned that the same solution procedure can be used for any dynamically developed velocity profiles and turbulent models in other conduit configurations such as channel geometries and rectangular, triangular or other tube sections. Different wall heating conditions, and viscous and other flows conditions could also be evaluated for different heating effects.

Acknowledgements The authors declare that they have no conflicts of interest in conducting work to any organisation or funding bodies. The authors would like to thank the reviewers for their valuable comments.

Compliance with ethical standards

Conflict of interest The authors declares there is no conflict of interest.

References

1. Cagin, S., Fischer, X., Delacourt, E., Bourabaa, N., Morin, C., Coutellier, D., Carre, B., Loume, S.: A new reduced model of scavenging to optimize cylinder design. *Simul T. Soc. Mod. Sim.* **92**(6), 1–14 (2016)
2. Cagin, S., Bourabaa, N., Delacourt, E., Morin, C., Fischer, X., Coutellier, D., Carré, B., Loumé, S.: Scavenging process analysis in a 2-stroke engine by CFD approach for a parametric 0D model development. *J. Appl. Fluid. Mech.* **9**(1), 69–80 (2016)
3. Choi, H., Moin, P.: Effects of the computational time step on numerical solutions of turbulent flow. *J. Comp. Phys.* **113**, 1–4 (1994)
4. García, M., Duque, J., Pierre, B., Figueroa, P.: Computational steering of CFD simulations using a grid computing environment. *Int. J. Interact. Des. Manuf.* **9**(3), 235–245 (2015)
5. Cucinotta, F., Nigrelli, V., Sfravara, F.: Numerical prediction of ventilated planing flat plates for the design of air cavity ships. *Int. J. Interact. Des. Manuf.* **12**, 1–12 (2017)
6. Cherrad, N., Benchabane, A.: Interactive process to control the evaporating temperature of refrigerant for solar adsorption cooling machine with new correlation. *Int. J. Interact. Des. Manuf.* **12**, 1–7 (2017)
7. Bahar, Y.N., Landrieu, J., Pére, C., Nicolle, C.: CAD data workflow toward the thermal simulation and visualization in virtual reality. *Int. J. Interact. Des. Manuf.* **8**(4), 283–292 (2014)
8. Amaya, A.F.D., Torres, A.G.D., Maya, D.A.A.: First and second thermodynamic law analyses applied to spark ignition engines modelling and emissions prediction. *Int. J. Interact. Des. Manuf.* **10**(4), 401–415 (2016)
9. Zhang, W., Cheng, C., Du, X., Chen, X.: Experiment and simulation of milling temperature field on hardened steel die with sinusoidal surface. *Int. J. Interact. Des. Manuf.* **12**, 1–9 (2017)
10. Afzal, N.: Wake layer in a thermal turbulent boundary layer with pressure gradient. *Heat Mass Transf.* **35**(4), 281–288 (1999)
11. Gbadebo, S.A., Said, S.A.M., Habib, M.A.: Average Nusselt number correlation in the thermal entrance region of steady and pulsating turbulent pipe flows. *Heat Mass Transf.* **35**(5), 377–381 (1999)
12. Yan, B.H., Gu, H.Y., Yu, L.: Numerical research of turbulent heat transfer in rectangular channels in ocean environment. *Heat Mass Transf.* **47**(7), 821–831 (2011)
13. Yan, B.H., Yu, Y.Q., Gu, H.Y., Yang, Y.H., Yu, L.: Simulation of turbulent flow and heat transfer in channels between rod bundles. *Heat Mass Transf.* **47**(3), 343–349 (2011)
14. Weigand, B., Wrona, F.: The extended Graetz problem with piecewise constant wall heat flux for laminar and turbulent flows inside concentric annuli. *Heat Mass Transf.* **39**(4), 313–320 (2003)
15. Habib, M.A., Attya, A.M., Said, S.A.M., Eid, A.I., Aly, A.Z.: Heat transfer characteristics and Nusselt number correlation of turbulent pulsating pipe air flows. *Heat Mass Transf.* **40**(3–4), 307–318 (2004)
16. Hui, G., Liejin, G.: Numerical investigation of developing turbulent flow in a helical square duct with large curvature. *J. Therm. Sci.* **10**(1), 1–6 (2001)
17. Roy, G., Vo-Ngoc, D., Bravine, V.: A numerical analysis of turbulent compressible radial channel flow with particular reference to pneumatic controllers. *J. Therm. Sci.* **13**(1), 24–29 (2004)
18. Eiamsa-ard, S., Changcharoen, W.: Analysis of turbulent heat transfer and fluid flow in channels with various ribbed internal surfaces. *J. Therm. Sci.* **20**(3), 260–267 (2011)
19. Taler, D.: Simple power-type heat transfer correlations for turbulent pipe flow in tubes. *J. Therm. Sci.* **26**(4), 339–348 (2017)
20. Tian, R., Dai, X., Wang, D., Shi, L.: Study of variable turbulent Prandtl number model for heat transfer to supercritical fluids in vertical tubes. *J. Therm. Sci.* **27**(3), 213–222 (2018)
21. Taler, D.: A new heat transfer correlation for transition and turbulent fluid flow in tubes. *Int. J. Therm. Sci.* **108**(2016), 108–122 (2016)
22. Belhocine, A., Wan Omar, W.Z.: Numerical study of heat convective mass transfer in a fully developed laminar flow with constant wall temperature. *Case Stud. Therm. Eng.* **6**, 116–127 (2015)
23. Belhocine, A.: Numerical study of heat transfer in fully developed laminar flow inside a circular tube. *Int. J. Adv. Manuf. Technol.* **85**(9), 2681–2692 (2016)
24. Belhocine, A., Wan Omar, W.Z.: Exact Graetz problem solution by using hypergeometric function. *Int. J. Heat Technol.* **35**(2), 347–353 (2017)
25. Belhocine, A., Abdullah, O.I.: Similarity and numerical analysis of the generalized Levêque problem to predict the thermal boundary layer. *Int. J. Interact. Des. Manuf.* **12**(3), 235–245 (2018)
26. Bryant, D.B., Sparrow, E.M., Gorman, J.M.: Turbulent pipe flow in the presence of centerline velocity overshoot and wall-shear under-shoot. *Int. J. Therm. Sci.* **125**, 218–230 (2018)
27. Wilcox, D.C.: *Turbulence Modeling for CFD*, 2nd edn. DCW Industries, La Canada (1998)
28. Kays, W.M., Crawford, M.E.: *Convective Heat and Mass Transfer*, 3rd edn. McGraw-Hill, New York (1993)

Publisher's Note Springer Nature remains neutral with regard to jurisdictional claims in published maps and institutional affiliations.